Retrieval of Cloud Microphysical Parameters from 94-GHz Radar Doppler Power Spectra

DAVID M. BABB AND JOHANNES VERLINDE

Department of Meteorology, The Pennsylvania State University, University Park, Pennsylvania

BRUCE A. ALBRECHT

Rosenstiel School of Marine and Atmospheric Science/MPO, University of Miami, Miami, Florida

(Manuscript received 12 March 1998, in final form 24 June 1998)

ABSTRACT

A technique is presented that uses Doppler spectra collected from a vertically pointing 94-GHz radar to reconstruct cloud and precipitation drop size distributions. A conceptual model describing the broadening of Doppler spectra by turbulence was adapted from earlier works presented in the literature. This model was then used as a basis for an algorithm that solves for parameters describing the turbulence and drop distribution. Numerically simulated Doppler spectra, calculated from known drop distributions, were first used to test the accuracy of the retrieval algorithm. The tests indicate that the retrieval algorithm can accurately retrieve the turbulence parameter and characteristic diameter but is less able to correctly determine the shape parameter. The technique was then applied to actual Doppler spectra collected from a liquid-phase stratus cloud. Vertical profiles of cloud properties such as liquid water content (LWC), effective radius, total number concentration, and mean vertical wind were obtained. The LWC profiles compared well with concurrent aircraft observations both in magnitude and profile shape. Integrated liquid water path agreed with microwave radiometer observations. A discussion is also presented on the limitations of the retrieval algorithm and the feasibility of retrieving cloud microphysical properties in a variety of situations.

1. Introduction

A significant problem encountered in the understanding of cloud processes is the routine measurement of cloud physical properties. Of these, the cloud drop size distribution is of fundamental interest. The cloud drop distribution determines the cloud radiative properties, and knowledge of its evolution is necessary if precipitation processes are to be understood.

Currently, our knowledge of cloud and precipitation drop distributions exists almost entirely from in situ measurements—the majority coming from aircraft observations using laser probes (Knollenberg 1970, 1981). While these measurements contributed greatly to our understanding of cloud processes, they have some inherent limitations: 1) a very small sampling volume, 2) samples at the same location separated by significant amounts of time (determined by the time it takes the aircraft to return to that location), and 3) a lack of instantaneous profiles of drop distributions.

For several problems, it is highly desirable to have high-resolution, vertical profiles of cloud properties. This is especially true when studying stratiform cloud processes. These observations can be obtained from aircraft only at great expense. However, recent advances in ground-based remote-sensing instrumentation and retrieval techniques are opening new opportunities to obtain such observations. In this paper, we present a technique to retrieve vertical profiles of cloud drop size distributions at high temporal and spatial resolutions using a millimeter-wave radar. In addition to the high sampling resolution, the radar can also be deployed for extended periods at low cost, thereby enabling the collection of large datasets from which statistics can easily be computed. These advantages suggest that a vertically pointing cloud radar can be a valuable tool in advancing our understanding of cloud microstructure and processes.

Millimeter-wave radar have long been recognized as having the potential to play an essential role in obtaining measurements of nonprecipitating clouds (e.g., Petrocchi and Paulson 1966). These radar observations have

Corresponding author address: David M. Babb, 503 Walker Bldg., University Park, PA 16802.
E-mail: dbabb@essc.psu.edu

been used to augment other surface-based remote-sensing instruments and to provide general cloud characteristics, such as location, thickness, and structure (e.g., Hobbs et al. 1985; Lhermitte 1987a,b; Peters et al. 1993; Syrett et al. 1995; Albrecht et al. 1995). To retrieve cloud microphysics using millimeter cloud radars, there have generally been two approaches: 1) using polarimetric parameters and 2) measuring the moments of the Doppler spectrum via pulsed-pair processing. Polarimetric techniques (e.g., Pasqualucci et al. 1983; Pazmany et al. 1994) are more suited for ice-phase or mixed-phase clouds due to the nonspherical shape of the hydrometeors. Techniques that use the Doppler moments have been shown to work well for liquid-phase boundary layer stratus clouds (e.g., Frisch et al. 1995a,b; Sassen and Liao 1996; Fox and Illingworth 1997) but require strict assumptions about cloud environment (e.g., vertical wind) and the state of the drop distribution (i.e., the nonexistence of drizzle) to retrieve the desired microphysical parameters.

Recent advancements in millimeter-wave signal processing hardware, including processor speed and storage capability, are allowing a third approach to obtain cloud microphysics. These advancements now enable one to compute the complete radar Doppler power spectrum in real time. This Doppler spectrum is a measure of power per unit phase shift—a phase shift caused by the motions (along the vertically pointing radar beam) of the scatters within the illuminated volume. With the assumption that fall velocity is a function of drop size, the power spectrum is intimately related to the drop size distribution.

Unfortunately, this relationship is not straightforward. The measured velocities of the cloud drops are the sum of their quiet-air fall velocity and ambient air motions. These unknown air motions can be divided into the volume-mean and turbulent components. The mean wind acts on all scatters equally, thus displacing the entire spectrum along the velocity axis. Conversely, the turbulent component of the vertical wind varies over the extent of the radar volume and tends to broaden the Doppler spectrum. This broadening occurs because similar size drops at different locations within the radar volume experience different turbulent contributions and, hence, have different perceived fall velocities.

The unknown air motions significantly impact the retrieval of microphysical parameters from radar measurements. For example, cloud drop distributions are frequently approximated using a three-parameter analytical function (e.g., modified gamma, Deirmendjian 1969; lognormal, Willis 1984). Furthermore, at least two additional variables are needed to describe the unknown air motion contributions. Therefore, the conventional, three-moment radar measurements (integrated reflectivity, mean reflectivity-weighted Doppler velocity, and spectrum width) are insufficient to solve this system of five unknowns.

Different approaches have been taken to account for the contributions of the mean and turbulent wind on vertically pointing radar measurements. The first group of these relied on estimation of the vertical mean wind contribution (e.g., Battan 1964; Rogers 1964). Others reduced the number of unknowns to three by assuming a two-parameter drop size distribution and a negligible turbulent contribution (e.g., Hauser and Amayenc 1981; Hauser and Amayenc 1983). This approach yielded reasonable results, but the assumptions restrict application to precipitation. A third method used direct measurement of the mean wind with a VHF Doppler radar (e.g., Fukao et al. 1985c; Wakasugi et al. 1985). Wakasugi et al. (1987) also considered the impact of turbulence on the retrievals, thus including all contributions. However, the long wavelength VHF radar ($\sim$6.5 m) is not sensitive enough to detect cloud (as opposed to precipitation) returns and, hence, cannot address the issue of cloud drop distributions.

Subsequent studies (Gossard 1988; Gossard and Strauch 1989; Gossard et al. 1990; Gossard 1994) further improved the technique presented by Wakasugi, using a shorter wavelength radar ($\sim$0.33 m). However, Gossard commented that the retrieved distributions are more representative of drizzle than cloud drops. He noted that the clear-air return contaminated the cloud spectral peak and suggested that a millimeter-wave radar would be better suited because the droplet backscatter far exceeds the clear-air return. In a more recent study, Gossard et al. (1997) applied their drop distribution retrieval method using a 35-GHz radar (8-mm wavelength). They show reasonable retrievals of cloud and drizzle drop distributions from marine stratocumulus. Unfortunately, there are no in situ observations for comparison.

In this paper, we will demonstrate a variation of Gossard's drop distribution retrieval algorithm using a 94-GHz (3 mm) radar with a very high spectral velocity resolution (0.031 25 m s^{-1}). To demonstrate the advantages and limitations of this method, the algorithm will be tested using simulated data. Further demonstration of the technique will be performed on Doppler spectra collected during a radar–aircraft intercomparison experiment.

2. Methodology

A conceptual model of the effects of turbulent broadening on a Doppler spectrum can be constructed as follows. First, consider a monodispersed population of drops. In a quiet-air radar volume, such a distribution will produce a single, narrow spectral peak centered at the fall velocity of the drops—called the quiet-air spectral line. Now, if this drop population is embedded in a turbulent medium, drops within the radar volume will experience different vertical velocities depending on their exact location. This will broaden the spectral return from the quiet-air spectral line to a distribution resembling the distribution of the turbulent velocities (Fig. 1a). Finally, if one now assumes that the total drop size

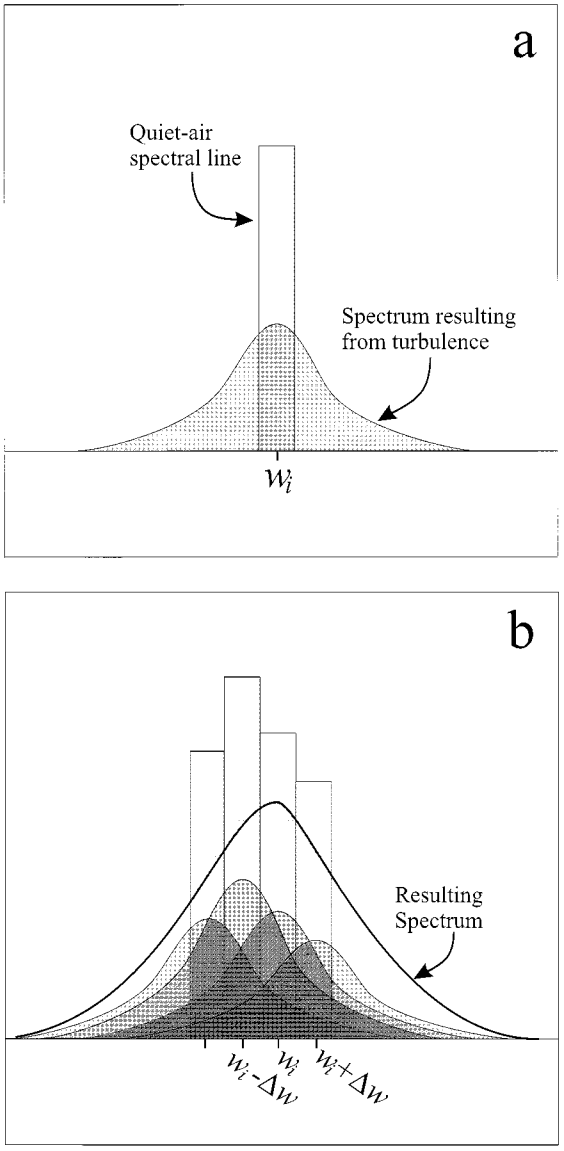

FIG. 1. Representation of the effect of turbulent broadening (a) on a single spectral line and (b) on a spectrum consisting of several spectral lines.

distribution is made up out of many such monodispersed distributions, each being broadened in a similar way, the final radar measured spectrum will be the sum of all the individually broadened spectra (Fig. 1b).

To demonstrate this idea mathematically, we first define a turbulence probability density function (PDF), following Gossard et al. (1997), as

$$P(w_i) = \frac{1}{\sqrt{\pi} w_\sigma} \exp\left[-\left(\frac{w_j - w_i}{w_\sigma}\right)^2\right], \quad (1)$$

where $P(dw)$ is the probability that drops with a quiet-air velocity of w_j will contribute to the spectral reflectivity between the velocities w_i and $w_i + dw$. The variable w_σ is the half-width of the distribution and represents the turbulent intensity.

To illustrate the effect of this turbulence PDF on a quiet-air spectrum, consider a quiet-air special function $S_Q(w)$. This function can be divided into intervals, each centered on a velocity w_i and having a width Δw. The quiet-air spectral reflectivity of each interval would then be $S_Q(w_i)\Delta w$. However, in the presence of turbulence, some of the drops with the quiet-air velocity w_i contribute to other velocity intervals ($w_i \pm n\Delta w$), thus reducing the measured spectral reflectivity at w_i. At the same time, drops from surrounding velocity intervals ($w_j \neq w_i$) contribute spectral reflectivity to the w_ith interval, as dictated by the PDF. In integral form, the relationship for determining the spectral reflectivity $[S_Z(w_i)\Delta w]$ at w_i can be written

$$S_Z(w_i)\Delta w = \frac{\Delta w}{\sqrt{\pi} w_\sigma} \int_{-\infty}^{0} S_Q(w_j) \exp\left[-\left(\frac{w_j - w_i}{w_\sigma}\right)^2\right] dw_j. \quad (2)$$

Following Gossard et al. (1990), we assume the drop distribution to be a modified gamma function of the form

$$N(D) = N_M \left(\frac{D}{D_M}\right)^\alpha \exp\left[(6 + \alpha)\left(1 - \frac{D}{D_M}\right)\right], \quad (3)$$

where α is the shape factor, and D_M and N_M are the reflectivity-modal drop diameter and number density per unit diameter, respectively, corresponding to the quiet-air spectral reflectivity peak (S_{QM}). Using the Rayleigh approximation for scattering from small water spheres, the above drop distribution can be transformed into a quiet-air, spectral reflectivity density as a function of drop diameter

$$S_Q(D) = S_{QM} \left(\frac{D}{D_M}\right)^{6+\alpha} \exp\left[(6 + \alpha)\left(1 - \frac{D}{D_M}\right)\right], \quad (4)$$

where S_{QM} is equal to $N_M D_M^6$ and has units of a spectral reflectivity density (e.g., $\text{mm}^6\ \text{m}^{-3}\ \mu\text{m}^{-1}$). Since we measure spectral reflectivity as a function of velocity, it is necessary to transform Eq. (4) into velocity space. Because the focus in this paper is on very small drops, it is appropriate to use the Stokes range, fall-velocity approximation $w \propto D^2$. The transformation results in the following:

$$S_Q(w_i) = \hat{S}_{QM} \left(\sqrt{\frac{w_i}{w_M}}\right)^{6+\alpha} \exp\left[(6 + \alpha)\left(1 - \sqrt{\frac{w_i}{w_M}}\right)\right], \quad (5)$$

where $\hat{S}_{QM}$ now has units of $[\text{mm}^6\ \text{m}^{-3}\ (\text{m s}^{-1})^{-1}]$.

Finally, by substituting Eq. (5) into Eq. (2) and letting $n = (6 + \alpha)$, we obtain

$$S_Z(w_i) = \frac{\hat{S}_{QM}}{\sqrt{\pi} w_\sigma} \exp\left[n - \frac{w_i^2}{w_\sigma^2}\right] \int_{-\infty}^{0} \left(\sqrt{\frac{w_j}{w_M}}\right)^n \exp\left[-\left(\frac{w_j}{w_\sigma}\right)^2 - n\sqrt{\frac{w_j}{w_M}} + \frac{2w_i w_j}{w_\sigma^2}\right] dw_j, \tag{6}$$

which is the equation that is used to characterize the spectra collected by the radar. This equation defines the spectral density as a function of four unknowns ($\hat{S}_{QM}$, w_M, w_σ, and α). However, with suitable assumptions, the number of unknowns can be reduced to three.

We first evaluate the function $S_Z(w_i)$ at w_M and solve for $\hat{S}_{QM}$. This gives

$$\hat{S}_{QM} = \frac{S_Z(w_M)}{\frac{1}{\sqrt{\pi} w_\sigma} \exp\left[n - \frac{w_M^2}{w_\sigma^2}\right] \int_{-\infty}^{0} \left(\sqrt{\frac{w_j}{w_M}}\right)^n \exp\left[-\left(\frac{w_j}{w_\sigma}\right)^2 - n\sqrt{\frac{w_j}{w_M}} + \frac{2w_M w_j}{w_\sigma^2}\right] dw_j}. \tag{7}$$

It was observed that at typical values of w_σ (~0.2 to 0.4 m s^{-1}), $S_Z(w_M)$ is approximately equal to the *observed* (as opposed to the quiet air) spectral reflectivity peak max[S_Z(obs)]. Using this fact and substituting Eq. (7) into Eq. (6) gives us

$$S_Z(w_i) = \max[S_Z(\text{obs})] \exp\left[\frac{w_M - w_i^2}{w_\sigma^2}\right] \frac{\int_{-\infty}^{0} \left(\sqrt{\frac{w_j}{w_M}}\right)^n \exp\left[-\left(\frac{w_j}{w_\sigma}\right)^2 - n\sqrt{\frac{w_j}{w_M}} + \frac{2w_i w_j}{w_\sigma^2}\right] dw_j}{\int_{-\infty}^{0} \left(\sqrt{\frac{w_j}{w_M}}\right)^n \exp\left[-\left(\frac{w_j}{w_\sigma}\right)^2 - n\sqrt{\frac{w_j}{w_M}} + \frac{2w_M w_j}{w_\sigma^2}\right] dw_j}, \tag{8}$$

which now is a function of only three unknowns (w_M, w_σ, and α).

In the preceding derivation, we have not accounted for the mean vertical wind. The cloud drops have fall velocities much smaller than the mean wind. Therefore, if the radar is sensitive enough to detect these cloud drops and has sufficient velocity resolution to resolve several points in the Doppler spectrum, then we can remove the mean vertical wind. This can be accomplished by shifting the cloud spectrum so that its maximum coincides with the first negative velocity bin. This procedure is supported by numerical simulations of radar spectra from known drop distributions using our available velocity resolutions. The simulations showed that the maximum of the cloud spectral peak is nearly always contained in the first downward velocity bin. The spectral data used in this study have a velocity resolution of 0.031 25 m s^{-1}. This resolution is sufficient to resolve several points on the cloud spectrum, and we are confident that the radar is sensitive enough to detect the cloud drops.

Once the mean wind is removed, the next step is to fit Eq. (8) to the observed spectrum. The fitting routine used to solve for the unknown variables uses a modified genetic algorithm (Eschelman and Schaffer 1993). A brief outline of the algorithm follows.

1) An initial ''population'' of solutions is generated from random initial values within the search criteria for the expected solution.
2) Each member of the population is evaluated using a cost function (described below) and given a fitness score.
3) The population is then allowed to ''breed.'' This breeding is accomplished by linear interpolation between two solutions in the present population. Combinations are statistically determined by the fitness score. A random ''mutation'' value is added to allow for hill climbing.
4) The new generation then becomes the population and the process is repeated.

This sequence is allowed to continue for a predetermined number of generations, with each generation more likely to contain an accurate solution. The final solution vector is determined by the population member with the highest fitness score after all generations have taken place.

The cost function for the genetic algorithm is the squared difference between Eq. (8) and the data. Multiple runs of the algorithm revealed that the retrieval of w_M is robust, but w_σ and α are highly variable. This variability was further investigated and was discovered

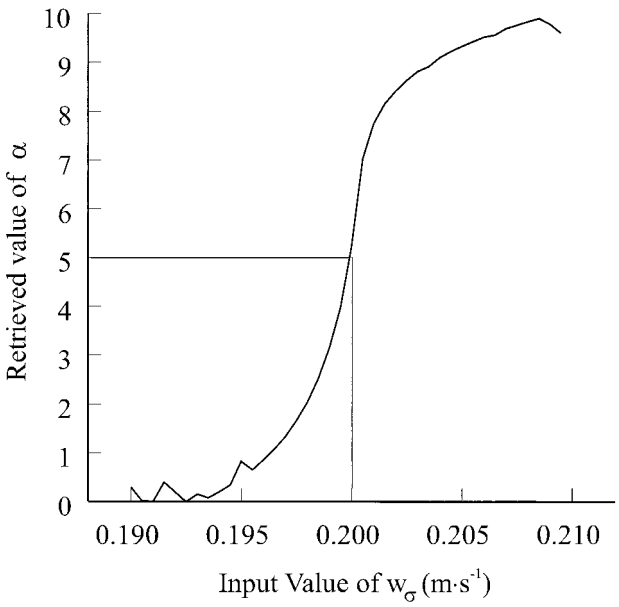

FIG. 2. The retrieved value of the shape parameter (α) as a function of the turbulent intensity (w_σ) during the phase II fitting process. The curve was constructed using simulated spectral data and the correct value of w_M. Correct values of α and w_σ are indicated by reference lines.

to result from a large dependence of α on the value of w_σ within the vicinity of the correct solution (Fig. 2). The curve in Fig. 2 was constructed by running the genetic algorithm multiple times on a simulated spectrum created from known w_M, w_σ, and α. For each run, the variable w_M was fixed at its correct value and w_σ, was fixed at various values surrounding its correct value (i.e., w_σ is used as the independent variable). Thus, the genetic algorithm was only solving for the single unknown (α). By examining the response of α to small errors in w_σ, we concluded that it is not possible to obtain w_σ with sufficient accuracy to retrieve α.

Therefore, the fitting procedure is conducted in three phases. In phase I, the genetic algorithm is used to solve for all three unknowns. The algorithm is repeated several times using different initial populations. The final solution vectors (w_M, w_σ, and α) from each run are then averaged. This average solution is deemed the best fit and is used as the initial guess in the phase II minimization process.

The phase II minimization is similar to the one used to create Fig. 2. The variable w_M retrieved from phase I is used in conjunction with a series of w_σ values that are centered on the phase I estimate. The genetic algorithm is used to solve for a value of α using a cost function that is the difference between the observed integrated reflectivity and the sixth moment of the calculated drop distribution (Z'). In terms of the variables of interest, this quantity can be written

$$Z' = 2S_{QM}w_M \exp(6 + \alpha)\frac{(7 + \alpha)!}{(6 + \alpha)^{\alpha+8}}, \qquad (9)$$

where S_{QM} is a function of all three variables [see Eq. (7)]. With each successive run of the algorithm, the value of w_σ is incremented and the retrieved value of α is recorded. As the value of w_σ passes through the correct value, the retrieved shape parameter goes from a lower asymptote less than one to an upper asymptote greater than 10. By selecting the w_σ that is centered on the interval over which α makes this transition, the value of w_σ can be retrieved to an accuracy of less than 5%.

In the third phase of the fitting routine, the retrievals of w_M and α are refined. This improvement is accomplished in a manner similar to phase I; however, this time the variable w_σ is held fixed at the value determined in phase II. By reducing the degrees of freedom, we found that there was a dramatic improvement in the retrieval of α. In addition, the retrieval confidence intervals for both w_M and α were significantly reduced.

3. Results

a. Retrievals of simulated spectra

Before the retrieval algorithm was applied to real Doppler spectra, it was tested in a controlled environment using simulated spectra. Such testing helps to determine the accuracy of the algorithm by providing the opportunity to compare the retrieved variables with the parameters used to create the input data. The simulated spectra were generated using Eq. (6) with known values of w_M, w_σ, α, and S_{QM}. Table 1 shows the range of values of these parameters tested. Also shown for reference are the corresponding microphysical observables calculated from the distribution in each case. The simulations were grouped into three categories, each testing the response of the retrieval algorithm to variations in w_M, w_σ, and α, respectively. The variable S_{QM} was held constant [5.0×10^{-4} mm^6 m^{-3} (m s^{-1})$^{-1}$] in all simulations.

The retrieved values of w_M, w_σ, and α from the simulated spectra are shown in Table 2. The values represent the mean solution for 60 runs of the genetic algorithm (phase III) using a 30-generation iteration and a population size of 120. The intervals shown with each retrieved variable are one standard deviation about the mean. Overall, the results demonstrate that the mean solutions of the retrieval algorithm can successfully determine the correct value of the unknown variables. Maximum mean-solution errors are generally within 10% for w_M, 5% for w_σ, and 20% for α. Confidence intervals were within a few percent for w_M, and w_σ but were considerably larger for α. Current work is focusing on the reduction of the confidence interval for α via improvements in the fitting routine.

Common microphysical observables such as liquid water content, effective radius, or maximum number density were also calculated from the simulations. The retrieved values (with their confidence intervals) are plotted in Figs. 3 a–c against the correct values (from Table 1). The graphs indicate that the liquid water con-

TABLE 1. List of parameters (w_M, w_σ, α) that created the simulated Doppler spectra used to test the retrieval algorithm. Also shown for reference are the corresponding values of commonly observed cloud properties: reflectivity modal diameter (D_M), modal diameter (D_o), modal number density (N_o), liquid water content (LWC), effective radius (R_e), and refelectivity (Z).

Simulation input			Cloud properties					
w_M	w_σ	α	D_M (μm)	D_o (μm)	N_o (m^{-3} μm^{-1})	LWC (gm^{-3})	R_e (μm)	Z (mm^6 m^{-3})
w_m dependence test								
−0.015	0.20	4	21.7	8.7	4.88	0.67	7.6	$1.32 \times 10^7/\times 10^{-5}$
−0.020	0.20	4	25.1	10.0	2.07	0.58	8.7	$1.76 \times 10^7/\times 10^{-5}$
−0.025	0.20	4	28.1	11.2	1.06	0.52	9.8	$2.15 \times 10^7/\times 10^{-5}$
−0.030	0.20	4	30.7	12.3	6.11	0.47	10.7	$2.64 \times 10^7/\times 10^{-5}$
w_σ dependence test								
−0.020	0.15	4	25.1	10.0	2.06	0.58	8.7	$1.76 \times 10^7/\times 10^{-5}$
−0.020	0.20	4	25.1	10.0	2.06	0.58	8.7	$1.76 \times 10^7/\times 10^{-5}$
−0.020	0.25	4	25.1	10.0	2.06	0.58	8.7	$1.76 \times 10^7/\times 10^{-5}$
−0.020	0.30	4	25.1	10.0	2.06	0.58	8.7	$1.76 \times 10^7/\times 10^{-5}$
α dependence test								
−0.020	0.20	3	25.1	8.4	2.99	0.62	8.4	$1.87 \times 10^7/\times 10^{-5}$
−0.020	0.20	4	25.1	10.0	2.07	0.58	8.7	$1.76 \times 10^7/\times 10^{-5}$
−0.020	0.20	5	25.1	11.4	1.57	0.55	9.1	$1.66 \times 10^7/\times 10^{-5}$
−0.020	0.20	6	25.1	12.5	1.26	0.52	9.4	$1.58 \times 10^7/\times 10^{-5}$

tent and effective radius values were retrieved within 10% of the correct values, and that maximum number density was determined to within a factor of 2. The exceptions are indicated by arrows in each figure. These two outlying cases will be addressed further in section 4a.

b. Retrievals of observed spectra

In addition to testing the retrieval algorithm on simulated data, the retrieval algorithm was applied to real Doppler spectra collected by The Pennsylvania State University 94-GHz Doppler radar (Albrecht et al. 1991; Miller and Albrecht 1995; Ackerman et al. 1993). The technical specifications for the radar as well as a complete discussion of the nonspectral signal processing can be found in Clothiaux et al. (1995). Peters et al. (1995) describe the technical specifications of the radar's spectral components.

The Doppler spectra profiles were collected on 6 April 1995 as part of a radar–aircraft intercomparison experiment. The profiles have a vertical resolution of 30 m and each 512-point spectrum consists of 60 incoherent averages resulting in a 6-s temporal resolution. Synoptic conditions indicated that the 200-m thick cloud, located at approximately 2 km, was associated with a slow-moving warm front approaching from the south. A sounding (Fig. 4) taken during the early observational period shows the temperature at cloud base to be about −3°C, and aircraft observations within the cloud layer indicate that the cloud consisted of only liquid hydrometeors. Inspection of the velocity-integrated reflectiv-

TABLE 2. Results of the retrieval algorithm tests. For each test, the parameters used to create the Doppler spectrum (left) are shown along with the retrieved parameters (right). Results are given by a mean solution and the std dev about that solution.

Simulation input			Range of retrieved values		
w_M	w_σ	α	w_m	w_σ	α
w_M dependence test					
−0.015	0.20	4	−0.0187 ± 0.0007	0.211 ± 0.004	8.0 ± 0.6
−0.020	0.20	4	−0.0203 ± 0.0006	0.207 ± 0.001	4.4 ± 0.4
−0.025	0.20	4	−0.0245 ± 0.0020	0.206 ± 0.00*	4.7 ± 2.0
−0.030	0.20	4	−0.0312 ± 0.0028	0.208 ± 0.003	6.6 ± 1.7
w_σ dependence test					
−0.020	0.15	4	−0.0197 ± 0.0001	0.160 ± 0.00*	5.0 ± 0.1
−0.020	0.20	4	−0.0203 ± 0.0006	0.207 ± 0.001	4.4 ± 0.4
−0.020	0.25	4	−0.0215 ± 0.0002	0.253 ± 0.00*	4.5 ± 0.3
−0.020	0.30	4	−0.0176 ± 0.0030	0.291 ± 0.003	3.0 ± 2.0
α dependence test					
−0.020	0.20	3	−0.0206 ± 0.008	0.207 ± 0.001	4.0 ± 0.5
−0.020	0.20	4	−0.0203 ± 0.0006	0.207 ± 0.001	4.4 ± 0.4
−0.020	0.20	5	−0.0208 ± 0.0008	0.207 ± 0.001	5.5 ± 0.4
−0.020	0.20	6	−0.0197 ± 0.0004	0.207 ± 0.002	4.8 ± 0.4

* Std dev less than 0.001.

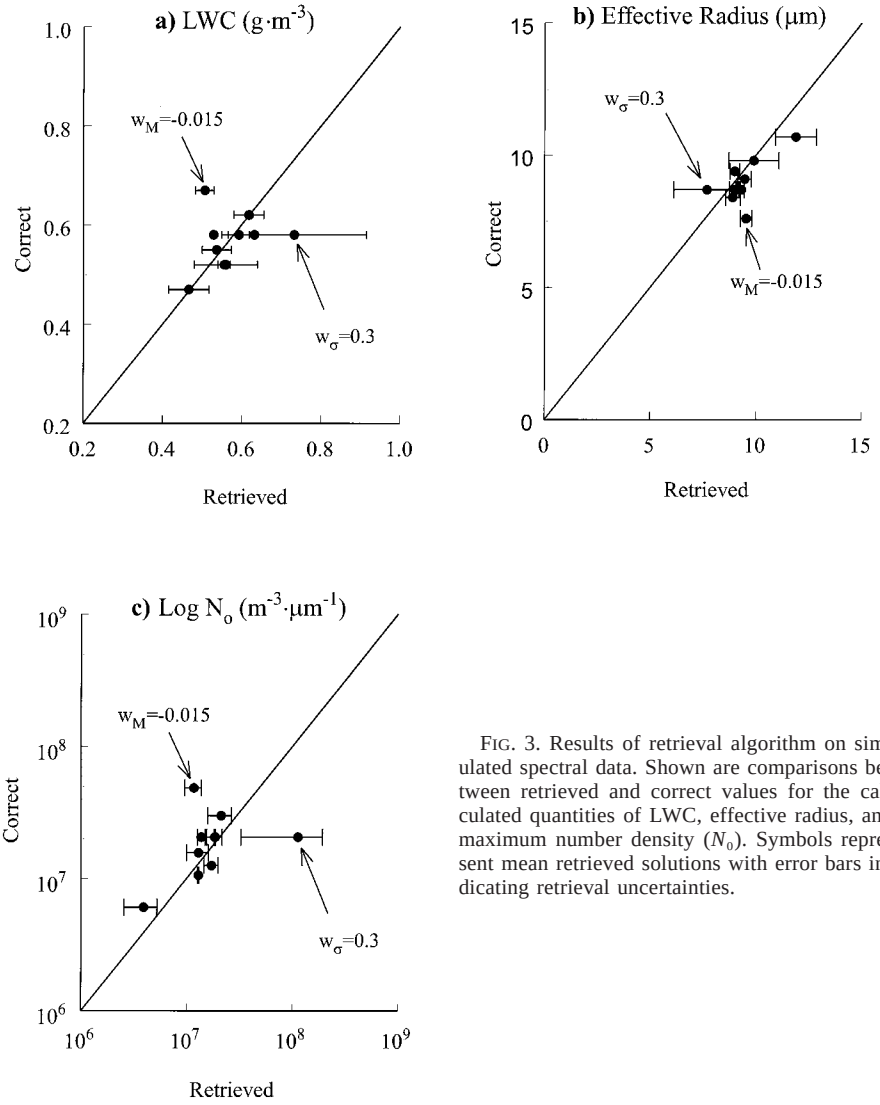

FIG. 3. Results of retrieval algorithm on simulated spectral data. Shown are comparisons between retrieved and correct values for the calculated quantities of LWC, effective radius, and maximum number density (N_0). Symbols represent mean retrieved solutions with error bars indicating retrieval uncertainties.

ity (Fig. 5) shows that there was no precipitation early in the observation period. Around 1150 UTC, the cloud began to thicken, and precipitation (although not reaching the ground) was evident. Spectrographs (a topographical view of a spectral profile) for the two periods (Figs. 6 and 7) reveal the presence of a large drop mode in the second profile that is absent in the earlier nonprecipitating profile.

The retrieval technique was applied to two profiles from the nonprecipitating period (1144:04 and 1144:31 UTC). Observables derived from the retrieval results for the two profiles are presented in Figs. 8 and 9. The solid line represents the mean solution, and the shaded region indicates retrieval uncertainty.

The mean vertical wind (Figs. 8a, 9a) increased through the depth of the cloud for both cases. At cloud top, the vertical velocity falls away as expected due to the stable layer above. Turbulent intensity (Figs. 8b, 9b) is seen to be higher in the center of the cloud with significant dropoffs at cloud base and cloud top. Values of w_σ range between 0.25 and 0.30 m s^{-1}, which are comparable to aircraft observations of vertical velocity that have been conditionally sampled to conform to the radar volume length scale.

Profiles of effective radius for the two cases (Figs. 8c, 9c) show no definitive trend with height. The total number concentration (Figs. 8d, 9d) increases through the depth of the cloud, reaches a maximum at approximately 75% of the depth of the cloud, and then decreases. Likewise, liquid water content (Figs. 8e, 9e) profiles have a similar shape. These profiles are reasonable given the weakly forced nature of this nonsurface-based stratus cloud.

As with any retrieval technique involving remotely sensed properties, it is imperative that the retrieved values be examined within the context of observations col-

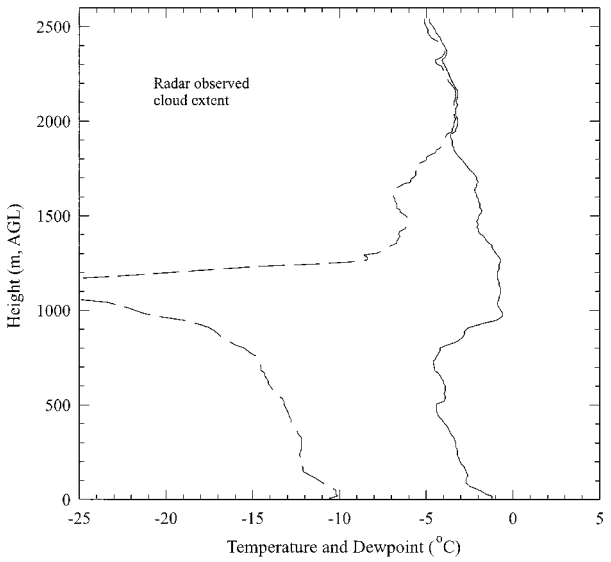

FIG. 4. Sounding from 1135 UTC 6 April 1995 with temperature (solid line) and dewpoint temperature (dashed line) profiles. Shading shows cloud extent as determined from radar observations.

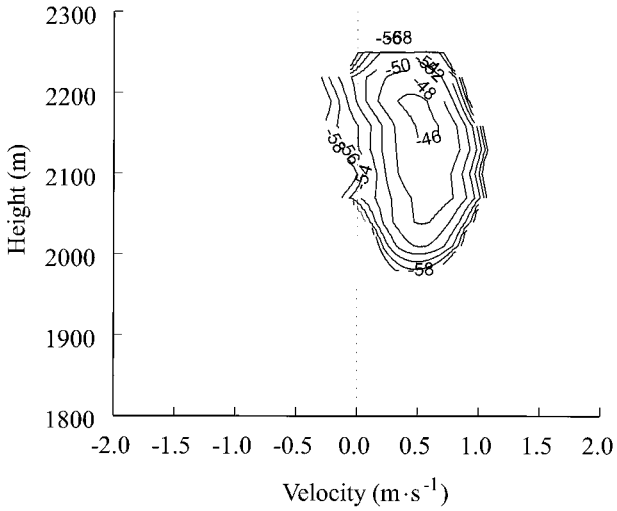

FIG. 6. A spectrograph taken from a nonprecipitating region of the cloud. Contour lines are levels of spectral reflectivity with units 10 $\log_{10}$ [mm^6 m^{-3} (m s^{-1})$^{-1}$].

lected from other instrument platforms—preferably those that provide in situ measurements. Therefore, we compare the results of our retrieval algorithm with cloud observations made from the University of Wyoming's instrumented aircraft and with a collocated microwave radiometer. We emphasize that these comparisons should not be used to judge the retrievals against some ''true'' value. Rather, such comparisons should be used to provide a framework of observational consistency given each instrument's unique sampling characteristics and limitations.

Aircraft FSSP (forward scattering spectrometer probe) observations (2–30 μm) of the drop distribution (and distribution-related parameters such as LWC) were collected during wind-parallel, level flight legs at various altitudes within the cloud. A comparison of the radar-retrieved LWC profiles with the aircraft observed LWC statistics is shown in Fig. 10. The aircraft data (1130–1215 UTC) were grouped into 25-m-height bins, and a mean value was calculated for each bin. To show the variation of observed liquid values, the standard deviation for each bin is also plotted. The comparison

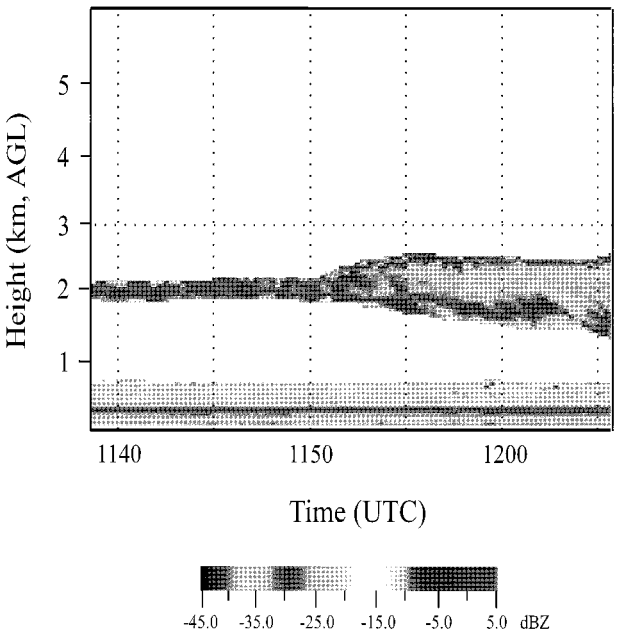

FIG. 5. Time–height profile of integrated reflectivity constructed from the vertically pointing 94-GHz radar.

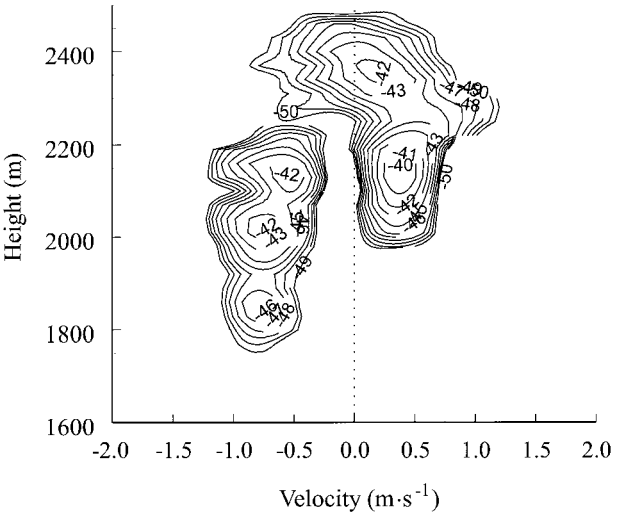

FIG. 7. As in Fig. 6 but during a drizzle event. Notice the large drop (higher velocity) signature falling from the cloud and evaporating before reaching the ground.

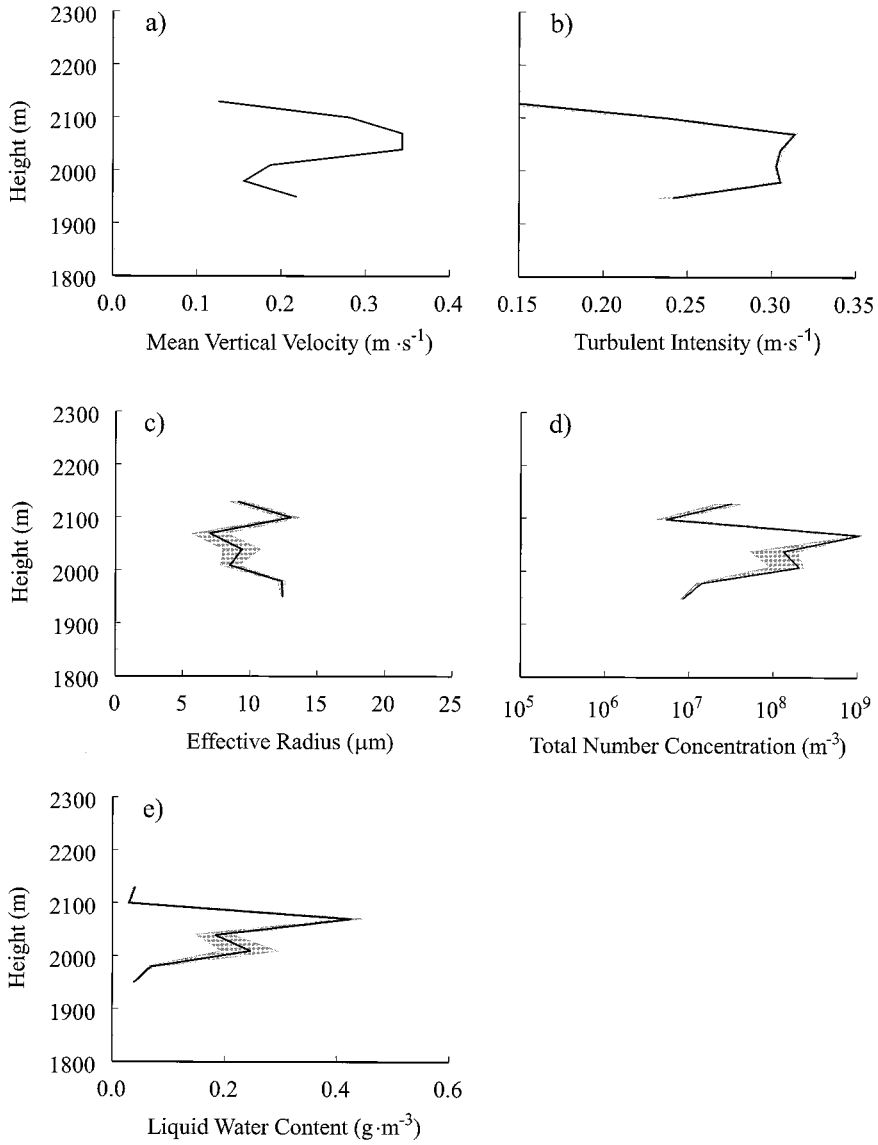

FIG. 8. Profiles of (a) mean vertical wind and (b) retrieved w_o for 1144:04 UTC. Also shown are profiles of (c) effective radius, (d) total number concentration, and (e) LWC calculated from the retrieved parameters. For each profile, the solid line represents the mean retrieved solution and the shading indicates retrieval uncertainty.

shows good agreement between the retrieved profiles and the aircraft data, especially for the 1144:31 UTC profile. Not only are the retrieved values within the natural variations observed by the aircraft but the shape of the mean liquid water profile is captured as well.

Current methods to remotely retrieve liquid water profiles in clouds use a *Z*–LWC relationship and require a priori knowledge of the total number concentration. To demonstrate the improvement in retrieving liquid water profiles using the spectrum fitting technique, two such *Z*–LWC relationships found in the literature are also plotted in Fig. 10. The dashed curves labeled with an ''F'' and an ''S'' are empirical *Z*–LWC formulas given by Frisch et al. (1995a) and Sassen and Liao (1996), respectively. In both cases the total number concentration used was 400 cm^{-3}. This value corresponded to the upper limit of total concentration observed by the aircraft's FSSP. It is clear from these curves that the empirical relationships are not capable of accurately describing the amount or shape of the LWC profile given an arbitrary reflectivity profile, even when the number concentration is specified with reasonable certainty.

By integrating the retrieved liquid water content values over the depth of the cloud, a total liquid water path can be obtained. For comparison, the retrieved liquid water paths are plotted with a time series of liquid water

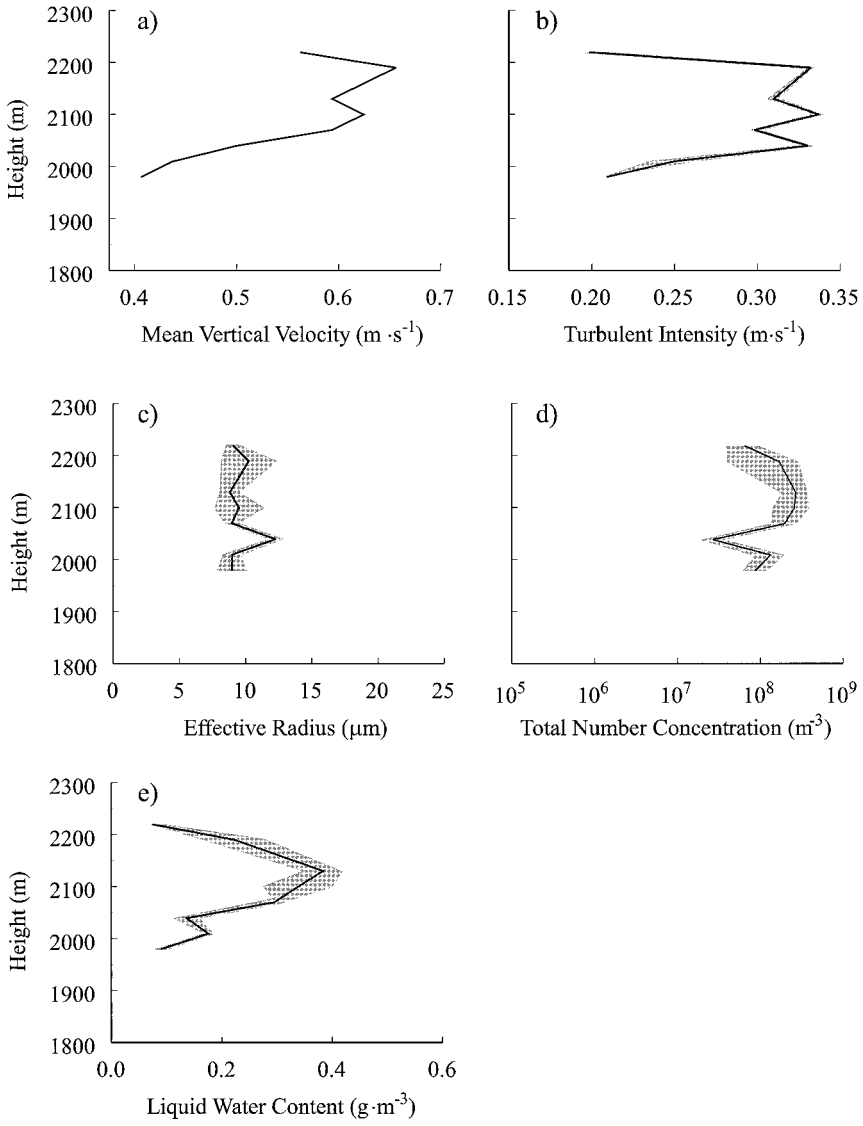

FIG. 9. As in Fig. 8 but for 1144:31 UTC.

path measured by a collocated microwave radiometer (Fig. 11). The figure shows that the values of the liquid water path retrieved from the radar are also in good agreement with the values observed by the radiometer. The discrepancy between the retrieved and observed liquid water paths at 1144:04 UTC is likely due to the differences in the field of view between the two instruments. The radiometer has a 2.5° field of view (compared with 0.25° for the radar) and will tend to average out the cloud inhomogeneities. However, when the cloud is relatively uniform (as around the 1144:37 UTC profile), the liquid water values agree well.

During testing of the retrieval algorithm, Doppler spectra from precipitation distributions were generated in addition to spectra from cloud drop distributions. These precipitation distributions appeared to be only minimally affected by turbulence of any intensity. After further investigation, we concluded that for large drops, the turbulence velocities are negligible compared with the cloud droplet fall speeds. This trend is a function of w_σ so that as the turbulent spectral width decreases, the drop diameter for which the retrieval algorithm is valid decreases.

Therefore, if the mean vertical wind can be resolved, then Doppler spectra with suitably large w_M's (e.g., >0.5 m s^{-1}) can simply be converted to number concentration using the appropriate *Z–N–D* relationship. Figure 12 shows several retrievals of the drizzle mode of the spectrum compared with aircraft PMS/1-DC probe observations from 1155:00 to 1200:00 UTC. The -50-dBZ line denotes the approximate maximum spectral sensitivity of the radar at 2 km.

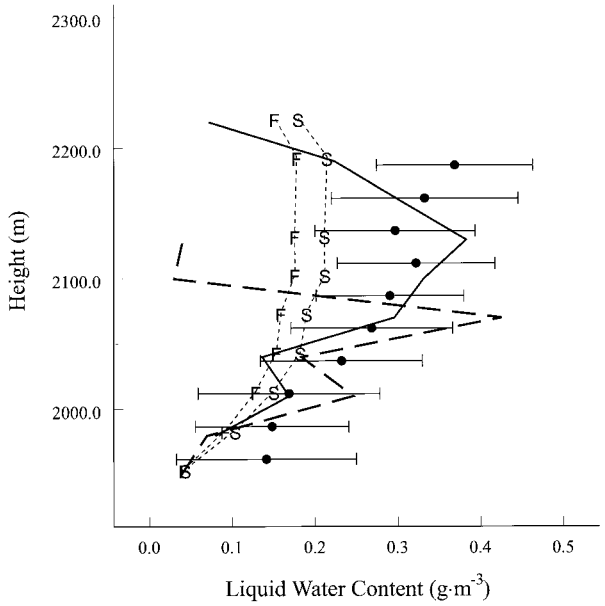

FIG. 10. Comparison of retrieved LWC profiles with aircraft observations. LWC profiles are from the 1144:04 (thick dashed line) and 1144:31 (solid line) retrievals. Aircraft observations of LWC (1130–1215 UTC) are grouped vertically into 25-m bins with symbols (●) representing mean values and error bars indicating the standard deviation of the observations. Also shown are two profiles (thin dashed lines) based on *Z*–LWC relationships presented by Frisch et al. (1995a) and Sassen and Liao (1996) (denoted by "F" and "S," respectively).

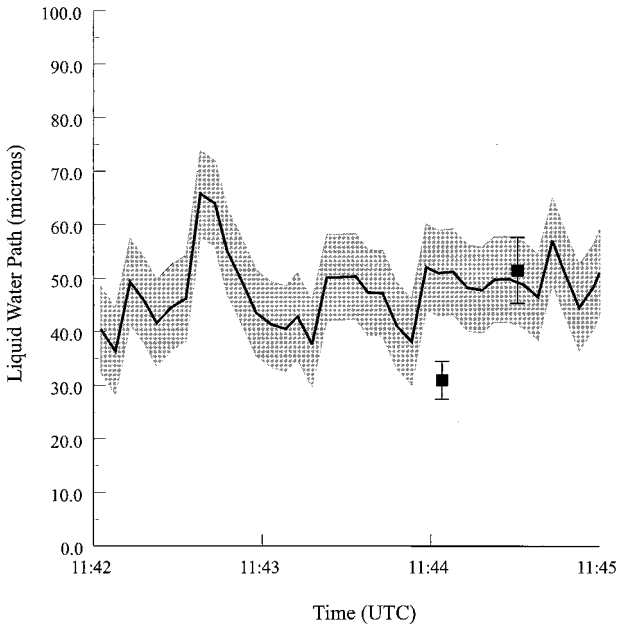

FIG. 11. Comparison of total liquid water path from a microwave radiometer (solid line) and retrieved profiles. Symbols (■) indicate mean retrieved values and error bars show retrieval uncertainties. The shaded area denotes the radiometer's random instrument error.

4. Discussion

As the results of the above section indicate, the retrieval routine can provide accurate estimates of drop distribution parameters. However, in this section we will discuss factors limiting the application of the retrieval algorithm. These factors can be divided into two categories: 1) inherent physical attributes of the turbulence and drop distribution and 2) data collection considerations.

a. Physical limiting factors

Several limitations of the algorithm were revealed by the simulated retrievals. These limitations are primarily a function of w_M and w_σ. The largest errors in the simulation tests were for the largest value of w_σ and the smallest value of w_M (Fig. 3). The reason for the degradation in retrieval accuracy can be seen by examining the ratio of S_Z to S_{QM} [see Eq. (6)]. Figure 13a shows this ratio as a function of both w_M and w_σ for a fixed value of α. Since the ratio of S_Z to S_{QM} describes the amount of turbulent broadening that has occurred, and hence how much drop information remains in the spectrum, this ratio can be used as an indicator of the retrieval algorithm accuracy (Gossard et al. 1997). As S_Z/S_{QM} goes to zero, it becomes increasingly difficult to retrieve a proper w_σ. This situation is most prominent

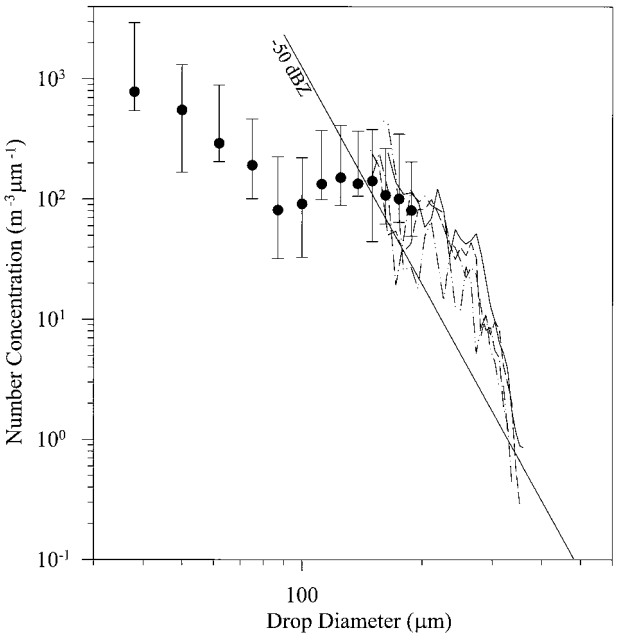

FIG. 12. Retrievals of the precipitation portion of the drop distribution (various lines). For comparison aircraft observations obtained from a 1-DC probe are also shown. Error bars denote maximum and minimum 1-DC concentrations with symbols indicating the mean concentrations. Also shown is the −50-dB*Z* contour as a function of the two axes, which represents the approximate maximum spectral sensitivity of the radar at 2 km.

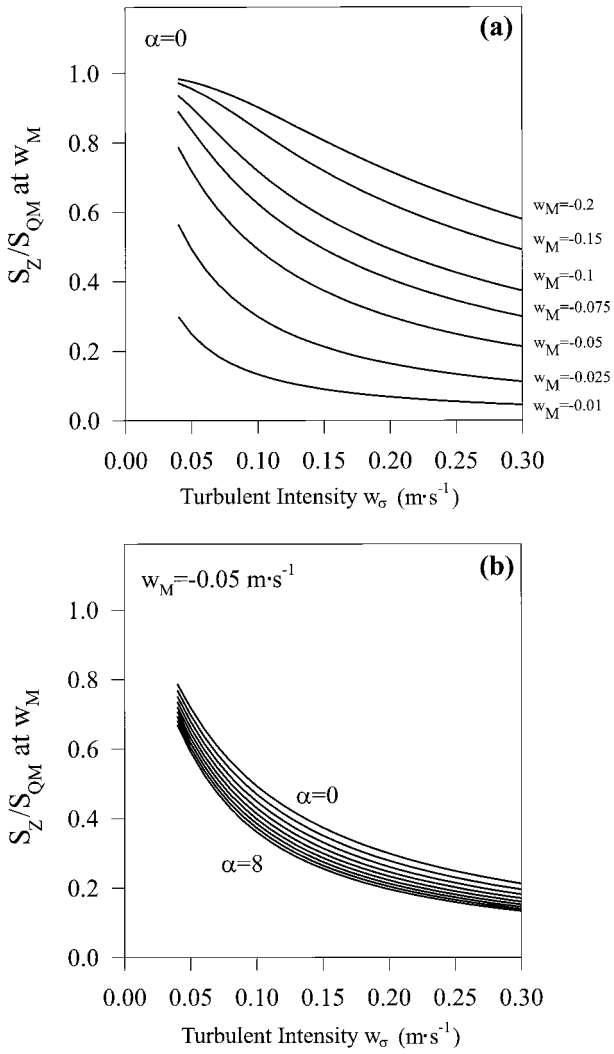

FIG. 13. Graphs showing the effects of turbulent broadening as a function of (a) w_M and (b) α. The ratio S_Z/S_{QM} at w_M is a measure of how much the quiet-air peak has been reduced as a result of turbulence.

for small values of w_M and large w_σ (Fig. 13a) and is enhanced further by increasing α (Fig. 13b).

Physically, this relationship between the accuracy of the retrieval technique and the magnitudes of w_M and w_σ is driven by the interplay of the turbulence and drop-size distribution contributions in the measured Doppler spectrum. Consider a population of drops falling in a turbulent medium. The ground-relative fall velocity of each drop is the sum of its quiet-air velocity and the local turbulent velocity. If the turbulent motions dominate the ground-relative fall velocity, the Doppler spectrum will simply resemble the velocity spectrum of the turbulence. In this extreme, the Doppler spectrum does not contain enough discernable information about the drop distribution due to the intensity of the turbulent fluctuations. This extreme can be realized in two possible ways: 1) very large turbulent fluctuations (indicated by large w_σ) and 2) very small drops (i.e., low fall velocities indicated by small w_M). In the simulated retrievals that failed, these conditions were met. Therefore, when implementing the retrieval routine, results that indicate a large turbulence value but have relatively small w_M's should be considered suspect.

Extrapolating this idea further, as w_M becomes increasingly smaller, there exists a point at which any turbulence contamination will prohibit an accurate retrieval. This point is the effective lower size limit for the retrieval algorithm given infinite spectral resolution. Simulations indicate that drop distributions with a reflectivity modal diameter (D_M) of less than 15 μm cannot be retrieved with this algorithm. With a finite spectral resolution, the minimum detectable diameter becomes a function of the velocity resolution of the Doppler spectrum as well. At our current maximum velocity resolution, we can retrieve distributions with a D_M of approximately 20 μm (a median diameter of $\sim$10 μm). Gossard et al. (1997), who use spectra with a considerable larger velocity resolution, indicate that their lower size limit is a drop distribution with $D_M \approx 40$ μm.

In addition to testing the retrieval algorithm with generated Doppler spectra, the effects of distribution bimodality were also investigated. Of particular interest were those cases where the drop modes were not sufficiently separated to produce distinct spectral features. We discovered that if a drop distribution is even slightly bimodal, then the second larger mode could completely dominate the Doppler spectrum due to turbulent broadening. This was true even if the smaller mode had a significantly higher concentration of drops.

For example, consider two drop distributions. The first distribution is bimodal and consists of a gamma-distributed cloud mode centered (D_o) at 8 μm and a second gamma-distributed intermediate mode located at 15 μm. The intermediate mode has a maximum number density (N_o) of half that of the cloud mode (Fig. 14a) but an LWC approximately eight times greater than the cloud mode. The second distribution consists of only the intermediate mode. When a Doppler spectrum is generated using the turbulence-broadening model, the cloud mode is completely lost in the intermediate mode's signal (i.e., the spectrum is identical to runs performed with no cloud mode) (Fig. 14b). This finding indicates that it may be impossible to resolve the smallest modes of multimodal cloud drop distributions.

To illustrate how this situation can occur in observed spectra, aircraft FSSP observations (mean, standard deviation, and total extent) are plotted along with two retrieved distributions (Fig. 15). The FSSP statistics are from a 15-min period around the profile times, and the profiles shown are from levels within 60 m of the aircraft altitude. In a situation analogous to the modeled case (Fig. 14), the retrieved distributions capture the shape of the FSSP measurements for drop sizes greater than 10 μm but not for sizes less than 10 μm. One can clearly see that the smallest mode of the distribution is not

represented. As we have shown, this error does not significantly affect the liquid water calculations since most of the liquid water is contained in the 20–30-μm drops. However, in situations where there are a large number of very small drops, the effective radius will be slightly overestimated. It is unknown at this time how this overestimation will impact cloud radiation budget estimates, but future work is planned to address this question.

b. Data collection considerations

In addition to the aforementioned considerations, certain care is needed in order to meet the observational criteria as well. Of primary importance is the fact that the cloud contain only liquid hydrometeors. This condition is the basis for all the reflectivity and velocity calculations used in the retrieval algorithm. Treatment of distributions containing ice particles will require more sophisticated algorithms that take crystal shapes and orientation into account.

A second concern when using the retrieval algorithm is the accuracy of the radar measurements. Errors in reflectivity calculations will not affect the retrieval of the unknown variables (i.e., w_M, w_σ, and α), but the quantities that involve the integrated reflectivity or number density (e.g., LWC) will be greatly affected. For example, a 3-dB error in measured reflectivity (an acceptable error tolerance for most radar) will result in a 50% error in LWC estimates. Therefore, a concerted effort should be made to obtain an accurate absolute calibration of the radar. The absolute calibration could also be verified using independent observations (e.g., aircraft, radiometer, etc.).

As stated earlier, the spectral profiles chosen to illustrate the retrieval technique were ''well behaved'' in the sense that they resembled spectra predicted by the turbulence-broadening model for unimodal drop distributions. However, observed spectra are usually multimodal, especially in cases involving precipitation processes. If the modes are separated, then it is a simple matter to obtain each distribution using the retrieval method appropriate for each spectral peak. If the modes overlap, then they must be separated, taking care to correctly apportion the proper spectral reflectivity to each peak. Preliminary tests indicate that it may be possible to extend the equations of the current conceptual model [Eqs. (3)–(8)] to include bimodal spectra. However, the introduction of several additional degrees of freedom into the optimization routine will likely create instability, thus requiring additional constraints.

5. Summary and conclusions

In this paper, we present a technique that reconstructs cloud and precipitation drop distributions using Doppler spectra collected from a vertically pointing 94-GHz radar. This technique is an adaptation of a scheme developed by Gossard (1988) and is based on a conceptual model describing the broadening of Doppler spectra by turbulence. This model was used as a framework for an algorithm in which the turbulence contamination is removed, leaving the quiet-air spectrum.

To study the accuracy and sensitivity of the retrieval algorithm, the technique was first tested with numerically simulated Doppler spectra calculated from known drop distributions. Results of these tests showed that the technique was capable of retrieving good estimates of the parameter values. The retrieved parameters were

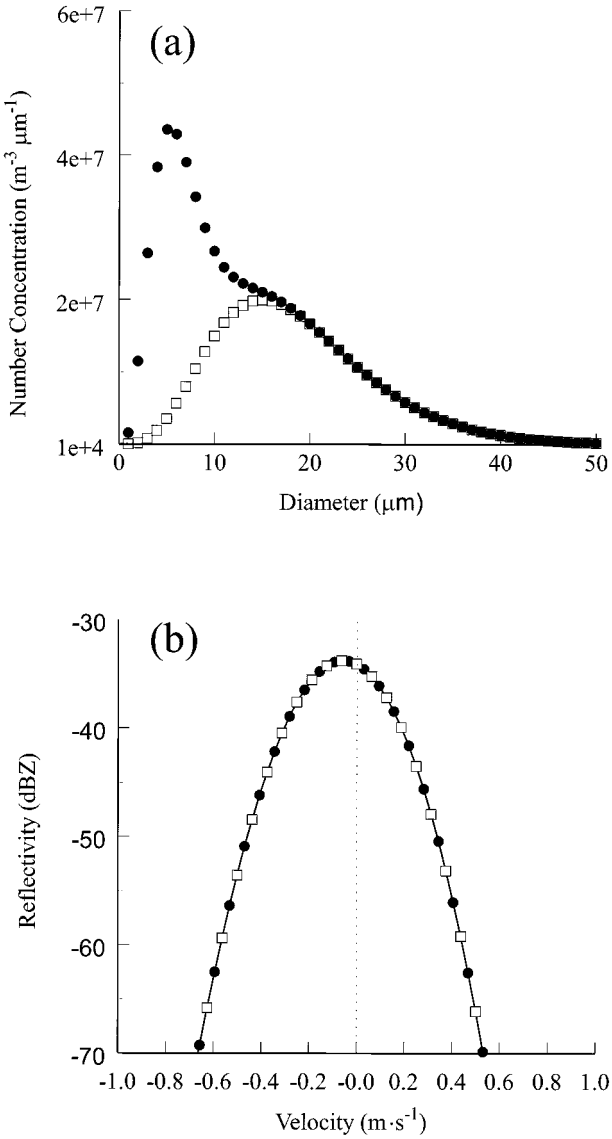

FIG. 14. Demonstration of how the presence of a larger intermediate cloud mode can mask the spectral contribution of the small cloud mode in the presence of turbulence. To illustrate this, Doppler power spectra are computed for two drop distributions. (a) The first distribution contains a small cloud mode and a slightly larger intermediate mode (●). The second distribution contains only the intermediate mode (□). (b) The resulting spectra are identical indicating that the cloud mode is not resolved.

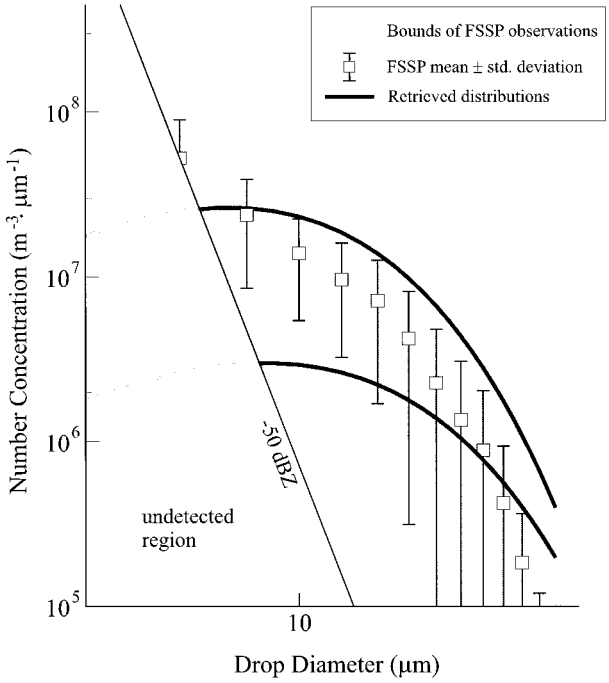

FIG. 15. Comparison between FSSP observed size distribution and retrieved distributions. Symbols (□) and error bars indicate mean and standard deviation, respectively, of FSSP concentration for each size bin over the sampling interval. The shaded region indicates the range of all FSSP observations over the sampling interval. The retrieved drop distributions are given by the two heavy, solid curves. As in Fig. 12, the −50-dBZ line is drawn to show which portions of the drop distribution are below the radar's sensitivity.

used to calculate commonly observed cloud variables (e.g., liquid water content) to study the effects of retrieval uncertainties on such quantities. The greatest uncertainties occurred when the turbulent intensity was large or the drop fall velocities are very small. This behavior indicates that drop information is lost if the turbulent fluctuations overwhelm the drops' quiet-air fall velocities. These findings also indicate that there is a minimum drop diameter for which turbulent contribution of any magnitude will mask the drop signature.

The technique was applied to Doppler spectra collected from a liquid-phase stratus cloud. Using the retrieval algorithm, vertical profiles of cloud properties such as LWC, modal diameter, and mean vertical wind were obtained. These profiles were consistent with what would be expected in a thin, nonprecipitating, warm-frontal stratus cloud and agreed well with concurrent observations from an aircraft and a microwave radiometer. We also showed that precipitation modes are not significantly affected by turbulence and can be retrieved directly from the Doppler spectra. Several precipitation drop distributions retrieved from spectra containing drizzle agreed well with size distributions observed by aircraft.

Application of this algorithm is limited by the requirements that 1) the cloud contains only liquid drops and 2) the radar is properly calibrated. In addition, multimodal cloud drop distributions may not be properly retrieved when the larger cloud modes dominate the total reflectivity. Finally, we stress that for such retrieval techniques to be credible there must be additional observations from other instrument platforms to provide a framework for judging the retrieval's effectiveness. These comparisons should also be performed in a variety of situations in order to clearly define the limitations of the technique.

Acknowledgments. We wish to acknowledge the contributions of George Young, who provided the genetic algorithm, Eugene Clothiaux, Natasha Miles, and the University of Wyoming King-Air flight crew. This work was partially funded under the following grants: ONR (#N00014-94-1-0681), NSF (#ATM9317371 and #ATM9629343), and DOE (#DE-F602-90ER61071).

REFERENCES

Ackerman, T. P., B. A. Albrecht, M. A. Miller, E. E. Clothiaux, R. M. Peters, and W. Syrett, 1993: Remote sensing of cloud properties using a 94-GHz radar. *Proc. Topical Symp. on Combined Optical-Microwave Earth and Atmosphere Sensing,* Albuquerque, NM, Amer. Meteor. Soc., 211–214.

Albrecht, B. A., T. P. Ackerman, G. G. Mace, D. W. Thomson, M. A. Miller, and R. M. Peters, 1991: A surface cloud observing system. Preprints, *Seventh Conf. on Meteological Observations and Instrumentation,* New Orleans, LA, Amer. Meteor. Soc., 443–446.

——, G. G. Mace, W. J. Syrett, and D. Thomas, 1995: Characteristics of continental stratus clouds from 94-GHz Doppler radar measurements. Preprints, *27th Conf. on Radar Meteorology,* Vail, CO, Amer. Meteor. Soc., 542–543.

Battan, L. J., 1964: Some observations of vertical velocities and precipitation sizes in a thunderstorm. *J. Appl. Meteor.,* **3,** 415–493.

Clothiaux, E. E., M. A. Miller, B. A. Albrecht, T. P. Ackerman, J. Verlinde, D. M. Babb, R. M. Peters, and W. J. Syrett, 1995: An evaluation of a 94-GHz radar for remote sensing of cloud properties. *J. Atmos. Oceanic Technol.,* **12,** 201–229.

Deirmendjian, D., 1969: *Electromagnetic Scattering on Spherical Polydispersions.* Elsevier, 290 pp.

Eschelman, L. J., and J. D. Schaffer, 1993: Real-coded genetic algorithms and interval-schemata. *Foundations of Genetic Algorithms 2,* L. D. Whitley, Ed., Morgan Kaufman, 187–202.

Fox, F. I., and A. J. Illingworth, 1997: The retrieval of stratocumulus cloud properties by ground-based cloud radar. *J. Appl. Meteor.,* **36,** 485–492.

Frisch, A. S., C. W. Fairall, and J. B. Snider, 1995a: On the measurement of stratus cloud and drizzle parameters in ASTEX with a Ka-band Doppler radar and a microwave radiometer. *J. Atmos. Sci.,* **52,** 2788–2799.

——, D. H. Lenschow, C. W. Fairall, W. H. Schubert, and J. S. Gibson, 1995b: Doppler radar measurements of turbulence in marine stratiform cloud during ASTEX. *J. Atmos. Sci.,* **52,** 2800–2808.

Fukao, S., K. Wakasugi, T. Sato, S. Morimoto, T. Tsuda, I. Hirota, I. Kimura, and S. Kato, 1985: Direct measurements of air and precipitation particle motion by VHF Doppler radar. *Nature,* **316,** 712–714.

Gossard, E. E., 1988: Measuring drop size distributions in cloud with clear-air sensing Doppler radar. *J. Atmos. Oceanic Technol.,* **5,** 640–649.

——, 1994: Measurement of cloud droplet spectra by Doppler radar. *J. Atmos. Oceanic Technol.,* **11,** 712–726.

——, and R. G. Strauch, 1989: Further guide for the retrieval of dropsize distributions in water clouds with a ground-based clear-air-sensing Doppler radar. Tech. Doc., NOAA/ERL/Wave Propagation Laboratory, Boulder, CO, 48 pp.

——, ——, and R. R. Rogers, 1990: Evolution of dropsize distributions in liquid precipitation observed by ground-based Doppler radar. *J. Atmos. Oceanic Technol.,* **7,** 815–828.

——, J. B. Snider, E. E. Clothiaux, B. Martner, J. S. Gibson, R. A. Kropfli, and A. S. Frisch, 1997: The potential of 8-mm radars for remotely sensing cloud drop size distributions. *J. Atmos. Oceanic Technol.,* **13,** 76–87.

Hauser, D., and P. Amayenc, 1981: A new method for deducing hydrometeor-size distributions and vertical air motions from Doppler radar measurements at vertical incidence. *J. Appl. Meteor.*, **20,** 547–555.

——, and ——, 1983: Exponential size distributions of raindrops and vertical air motions deduced from vertically pointing Doppler radar using a new method. *J. Climate Appl. Meteor.,* **22,** 407–418.

Hobbs, P. V., N. T. Funk, R. R. Weiss, J. D. Locatelli, and K. R. Biswas, 1985: Evaluation of 35-GHz radar for cloud physics research. *J. Atmos. Oceanic Technol.,* **2,** 35–48.

Knollenberg, R. G., 1970: The optical array: An alternative to scattering or extinction for airborne particle size determination. *J. Appl. Meteor.,* **9,** 86–103.

——, 1981: Techniques for probing cloud microstructure. *Clouds: Their Formation, Optical Properties, and Effects*, P. V. Hobbs and A. Depak, Eds., Academic Press, 15–19.

Lhermitte, R. M., 1987a: A 94-GHz Doppler radar for cloud observations. *J. Atmos. Oceanic Technol.,* **4,** 36–48.

——, 1987b: Small cumuli observed with a 3-mm wavelength Doppler radar. *Geophys. Res. Lett.,* **14,** 707–710.

Miller, M. A., and B. A. Albrecht, 1995: Surface-based observations of mesoscale cumulus–stratocumulus interactions during ASTEX. *J. Atmos. Sci.,* **52,** 2809–2826.

Pasqualucci, F., B. W. Bartram, R. A. Kropfli, and W. R. Moninger, 1983: A millimeter-wavelength dual-polarization Doppler radar for cloud and precipitation studies. *J. Climate Appl. Meteor.,* **22,** 758–765.

Pazmany, A., J. Mead, R. McIntosh, M. Hervig, R. Kelly, and G. Vali, 1994: 95-GHz polarimeteric radar measurements of orographic cap clouds. *J. Atmos. Oceanic Technol.,* **11,** 140–153.

Peters, R. M., B. A. Albrecht, and M. A. Miller, 1993: Marine boundary-layer profiling with a 94-GHz radar. *Proc. Eighth Symp. on Meteorological Observation and Instrumentation,* Anaheim, CA, Amer. Meteor. Soc., 467–472.

——, ——, G. G. Mace, T. P. Ackerman, D. M. Babb, and E. E. Clothiaux, 1995: Real-time spectral observations of clouds and precipitation using a 94-GHz radar. Preprints, *27th Conf. on Radar Meteorology,* Vail, CO, Amer. Meteor. Soc., 577–579.

Petrocchi, R. J., and W. H. Paulsen, 1966: Meteorological significance of vertical density profiles of clouds and precipitation obtained with the An/TPQ-11 radar. Preprints, *12th Conf. on Radar Meteorology*, Norman, OK, Amer. Meteor. Soc., 476–472.

Rogers, R. R., 1964: An extension of the *Z–R* relation for Doppler radar. Preprints, *11th Conf. on Radar Meteorology,* Boulder, CO, Amer. Meteor. Soc., 158–161.

Sassen, K., and L. Liao, 1996: Estimation of cloud content by W-band radar. *J. Appl. Meteor.,* **35,** 932–938.

Syrett, W. J., B. A. Albrecht, and E. E. Clothiaux, 1995: Vertical cloud structure in a midlatitude cyclone from a 94-GHz radar. *Mon. Wea. Rev.,* **123,** 3393–3407.

Wakasugi, K., S. Fukao, S. Kato, A. Mizutani, and M. Matsuo, 1985: Air and precipitation particle motions within a cold front measured by the MU VHF radar. *Radio Sci.,* **20,** 1233–1240.

——, A. Mizutani, M. Matsuo, S. Fukao, and S. Kato, 1987: Further discussion on deriving dropsize distribution and vertical air velocities directly from VHF Doppler radar spectra. *J. Atmos. Oceanic Technol.,* **4,** 170–179.

Willis, P. T., 1984: Functional fits to some observed drop size distributions and parameterization of rain. *J. Atmos. Sci.,* **41,** 1648–1661.